On the determination of absolute vibrational excitation probabilities in molecule-surface scattering: Case study of NO on Au(111)

Russell Cooper[*1], Zhisheng Li[2], Kai Golibrzuch[1], Christof Bartels[1], Igor Rahinov[3], Daniel J. Auerbach[4,5], Alec M. Wodtke[1,4,5]

[1]Institute for Physical Chemistry, Georg-August University of Göttingen, Göttingen, Germany
[2]Department of Chemistry, Columbia University
[3]Department of Natural Sciences, The Open University of Israel
[4]Department of Chemistry and Biochemistry, University of California Santa Barbara
[5]Max Planck Institute for Biophysical Chemistry, Göttingen, Germany

Abstract

We describe a method to obtain absolute vibrational excitation probabilities of molecules scattering from a surface based on measurements of the rotational state, scattering angle, and temporal distributions of the scattered molecules and apply this method to the vibrational excitation of NO scattering from Au(111). We report the absolute excitation probabilities to the v=1 and v=2 vibrational states , rotational excitation distributions, and final scattering angle distributions for a wide range of incidence energies and surface temperatures. In addition to demonstrating the methodology for obtaining absolute scattering probabilities, these results provide an excellent benchmark for theoretical calculations of molecule-surface scattering.

1. INTRODUCTION

A fundamental molecular level insight into the underlying dynamics of energy exchange between molecules and metal surfaces is a vital prerequisite to a comprehensive theory of gas-surface chemistry, bearing on subjects ranging from corrosion and electrochemistry to heterogeneous catalysis. The experimental evidence accumulated over more than two decades[1-18]

accompanied by powerful theoretical analysis[19-27] leave little doubt as to the existence of electronically nonadiabatic influences – Born-Oppenheimer Approximation (BOA) breakdown – on these energy transfer processes. Energy transfer between electron-hole pairs (EHP) in the metal and vibrational degrees of freedom (EHP-V) has received particular attention[4,5,9,12,20,21,24-26], as vibration is a degree of freedom coupling directly to the reaction coordinate.

Molecular beam–surface scattering experiments combined with laser based methods of preparation and detection enable control over orientation, velocity, and the internal state of the gaseous collision partner, and hence produce experimental results that can be directly compared to high-level theoretical calculations. The ample evidence of energy exchange between molecular vibrations and metallic EHPs gained from molecular beam-surface scattering experiments includes studies of (single and multi-quantum) vibrational excitation[8,9,12], (single and multi-quantum) vibrational relaxation[4,28] and electron emission[5,6,29] occurring in the course of molecule-surface encounters. Specifically, vibrational excitation exhibiting an Arrhenius-like surface temperature dependence with activation energy equal to the vibrational excitation energy is often considered to be a signature of electronically nonadiabatic behavior in molecule-surface encounters[7,10,12].

While the surface temperature dependence of vibrational excitation has been investigated in detail[10,12], the *absolute values* of vibrational excitation probability and the magnitude of the pre-exponent in Arrhenius surface temperature dependence received little attention until recently[7-9]. Disregarding the absolute values of vibrational excitation probability and focusing entirely on the temperature dependence is unfortunate since the magnitude of the pre-exponential coefficient provides information about the strength of electronically nonadiabatic coupling for a given molecule-surface system[1,7]. Very recently absolute vibrational excitation probabilities were

reported for single and multi-quantum vibrational excitation of NO scattered from Au(111)[9] and a state-to-state kinetic model was used to analyze and interpret the pre-exponential factors in Arrhenius-like surface temperature dependence and compare the intrinsic likelihood of EHP-V coupling for different EHP-mediated vibrational excitation events[1,7]. Furthermore, experiments examining the absolute probability of vibrational excitation provide a stringent test for the theories of electronically nonadiabatic interactions. The comparison of extensive absolute vibrational excitation probability data to predictions of perturbative electronic friction theory[22,24] and to independent electron surface hopping (IESH) theory[19] leaves little doubt that EHP-V coupling occurs via formation of transient negative ions[30].

Clearly, accurate measurement of absolute vibrational excitation probabilities over a wide range of incidence translational energies and surface temperatures is a mandatory prerequisite for such in-depth understanding of the EHP-V coupling mechanism. Measuring absolute excitation probabilities is a difficult task that requires various experimental factors to be taken into consideration: detector response, choice of a spectral band, knowledge of transition strengths, laser pulse energy dependence of the signal, angular and temporal distributions of the scattered molecules, velocity of the scattered molecules, etc. In this work we provide a detailed account of how these factors should be taken into consideration in evaluating absolute vibrational excitation probabilities by considering the case of NO colliding with Au(111) surface.

Specifically, the experimental protocol presented in this work is employed to determine absolute vibrational excitation probabilities for both the fundamental, NO(v=0→1), and first overtone transition, NO(v=0→2), when NO is scattered from a Au(111) surface at six different incidence energies, E_i, from 0.11eV to 1.05eV at surface temperatures, T_S, ranging from 300K to 1000K. These results provide an extensive benchmark dataset that probes the EHP-V coupling

for this system suitable for comparison with theories of electronically nonadiabatic interactions in molecule surface collisions. Furthermore, the experimental protocol described here should be applicable to the measurement of absolute transition probabilities for other systems.

2. EXPERIMENTAL METHODS

Our gas-surface scattering apparatus has been described previously in detail.[31] Supersonic molecular beams of NO are produced using a 10-Hz piezo-electrically driven pulsed valve. The translational energy distribution of the beams is adjusted by seeding NO in inert carrier gases with varying mass. See Table 1. The beam is skimmed, passed through two stages of differential pumping, and subsequently enters an ultra-high vacuum (UHV) scattering chamber where the NO molecules scatter from an Au(111) crystal at near normal incidence. A schematic of the machine is presented in Fig. 1. The Au(111) surface temperature can be varied, from room temperature to the melting point of the crystal, by resistive heating of tungsten wires to which the Au crystal is mounted. The scattering chamber has a base pressure of ~1.5 x 10^{-10} Torr, increasing to ~1 x 10^{-9} Torr with the molecular beam running. The Au(111) surface was cleaned by Argon ion bombardment, for ~1 hour, checked for contamination with Auger spectroscopy, and annealed for ~45 min. prior to scattering experiments. The sample is then cooled to room temperature before beginning scattering experiments. After scattering experiments the surface was again checked for contamination using Auger spectroscopy, with no major contamination found. The scattering chamber is equipped with optical ports allowing the use of UV (~ 230 nm) and IR (~1.8μm) laser beams[31], which are generated with Q-switched Nd:YAG-pumped dye lasers with appropriate frequency conversion schemes. The UV radiation is used for quantum state selective (1+1) REMPI ionization of scattered NO via $A^2\Sigma^+$ (v′)←$X^2\Pi$(v″) transistions,

known as the the $\gamma_{v',v''}$-bands. The ions are collected with ion optics (two-element cylindrical ion lens and repeller) and detected by a dual micro-channel plate detector (MCP). In many experiments there was a high ion background associated with heating the crystal. We believe this background stems from emission of K^+ ions from the W wires use to heat the Au(111) sample. The background was so high that it reduced the gain of the MCP detector. Since the background was CW, and the signal was pulsed, we pulsed the MCP so that it was only on during the time the signal was present. This reduced the gain depletion problem to acceptable levels. The magnitude of the voltage across the MCP was adjusted for each vibrational state such that the signal intensity was not saturated. To calibrate the relative MCP gain, the variation of a small ion signal was measured over the entire range of the MCP voltages used in this work, where the strength of the signal was chosen to avoid saturation at the highest gain (see Section 3).

To accurately determine the absolute vibrational excitation probabilities (as elaborated in detail in Section 3), spectral, angular (spatial) and temporal distributions of incident and scattered NO molecules must be recorded. By scanning the wavelength of the REMPI laser over the $A^2\Sigma^+$ ($v'=0$)←$X^2\Pi$($v''=0,1,2$) vibrational bands, rotationally resolved spectra of NO(v=0,1,2) in the incident and scattered beam were recorded (see Section 3b). The angular distributions of the scattered and incident beams were recorded by vertical translation of the REMPI laser beam in the plane perpendicular to the molecular beam (see Section 3c). The temporal distribution of the scattered and incident beams was measured by recording the REMPI signal at a variety of delays between the opening of the pulsed nozzle and firing of the REMPI laser (see Section 3d).

To quantify the degree of translational inelasticity and the translation-vibration (T-V) coupling required for flux-density corrections, accurate high resolution measurements of incident

and scattered velocity distributions are required. IR-UV double resonance is used for accurate velocity measurements of the molecular beams.[32,33] The velocities of the incident and scattered molecules were obtained from the analysis of time-of-flight spectra measured by state-specific ionization of NO tagged via vibrational overtone pumping by an IR laser a known distance from the UV laser beam used for REMPI detection.

3. RESULTS

A. Overview of experimental principles

In this work, we report absolute vibrational excitation probabilities, $P_{0\text{-}v}$, for NO(0→v) transitions resulting from collisions with the (111) surface of solid gold. Below we describe the derivation of $P_{0\text{-}v}$ from laboratory observations of REMPI signal strengths. For the conditions of single-bounce direct scattering, $P_{0\text{-}v}$ is defined as the ratio of scattered molecules in state v to all scattered molecules

$$P_{0-\mathrm{v}} \equiv \frac{N_\mathrm{v}}{\sum_i N_i} \qquad (1),$$

For the case where almost all NO molecules are initially in v=0 and when the sum of the vibrational excitation probabilities is much less than unity, as in this work, Eq. (1) can be simplified as follows,

$$P_{0-\mathrm{v}} \cong \frac{N_\mathrm{v}}{N_0} \equiv \frac{\text{Number of scattered molecules in state v}}{\text{Number of scattered molecules in v} = 0} \qquad (2)$$

Thus, by determining the ratio of N_v to N_0, we obtain absolute vibrational excitation probabilities.

The practical requirements for implementing this conceptually simple strategy are, however, rather complicated. Specifically, we require vibrational state specific information on scattered molecules, such as scattering angular, $\Theta_v(\theta)$, and rotational population, $n_v(j)$, distributions. Here θ represents the scattering angle with respect to the surface normal, j represents the rotational quantum numbers of the scattered molecules in vibrational state v probed by the (1+1) REMPI detection scheme. In general, one also needs rotational line strengths, $S(j_\Sigma, j)$, and Franck-Condon factors, $Q(v_\Sigma, v)$, for the resonant $A^2\Sigma^+(v')\leftarrow X^2\Pi(v'')$ transition of NO. Here, j_Σ and v_Σ represent the rotational and vibrational quantum numbers, respectively, of the intermediate, electronically-excited $A^2\Sigma^+(v')$ state used in the (1+1) REMPI scheme. We must also consider the wavelength dependent ionization cross-section of the intermediate, electronically-excited $A^2\Sigma^+(v')$ state, $\sigma_{v_\Sigma}(\lambda_{MPI,v})$, where $\lambda_{MPI,v}$ is the laser wavelength used to detect state v via state v_Σ by REMPI. The REMPI signal also depends on the time delay, τ, between the opening of the pulsed valve and the firing of the pulsed detection laser. This is described by a time dependent function, $\Delta_v(\tau)$. This function may be different for each vibrational channel as the average velocity, $\langle u_v \rangle$, of the scattered molecules depends on the final vibrational state. The time delay between opening of the pulsed nozzle and firing the detection laser, τ_v, and the angle with respect to the surface normal, θ_v, may be chosen differently for each v-state probed, for reasons of convenience, as will be explained in the following sections. Table 2 provides an overview of the functions and variables given in this paragraph.

Noting that REMPI signals are proportional to molecular density, are a function of the laser pulse energy, $f(I_v)$, and the MCP gain, Γ_v, we arrive at a relationship between REMPI signal strength, $SIG_v(j_\Sigma, j)$, and $n_v(j)$, shown below.

$$\mathrm{SIG_v}(j_\Sigma, j, \theta_\mathrm{v}, \tau_\mathrm{v})$$

$$\propto \frac{n_\mathrm{v}(j)}{\langle u_\mathrm{v}\rangle} \times S(j_\Sigma, j) \times \Theta_\mathrm{v}(\theta_\mathrm{v}) \times Q(\mathrm{v}_\Sigma, \mathrm{v}) \times \sigma_{\mathrm{v}\Sigma}\left(\lambda_{MPI,\mathrm{v}}\right) \times \Delta_\mathrm{v}(\tau_\mathrm{v}) \times \Gamma_\mathrm{v} \times f(I_\mathrm{v}) \quad (3)$$

Although the laser power is not constant over the entire range, the variation was small (<10%) and thus could be ignored in our experiments.

Here, dividing by the average velocity of the scattered molecules, $\langle u_\mathrm{v}\rangle$, is used for the density-to-flux conversion.[34] θ_v and τ_v are chosen to maximize the signal and minimize background, such as signal arising from the incident beam.

We can invert Eq. (3) as follows:

$$n_\mathrm{v}(j) \propto \frac{\mathrm{SIG_v}(j_\Sigma, j, \theta_\mathrm{v}, \tau_\mathrm{v}) \times \langle u_\mathrm{v}\rangle}{S(j_\Sigma, j) \times \Theta_\mathrm{v}(\theta_\mathrm{v}) \times Q(\mathrm{v}_\Sigma, \mathrm{v}) \times \sigma_{\mathrm{v}\Sigma}\left(\lambda_{MPI,\mathrm{v}}\right) \times \Delta_\mathrm{v}(\tau_\mathrm{v}) \times \Gamma_\mathrm{v} \times f(I_\mathrm{v})} \quad (4)$$

To obtain N_v, we must sum over the populations of all rotational states, j.

$$N_\mathrm{v} = \sum_j n_\mathrm{v}(j)$$

$$\propto \sum_j \frac{\mathrm{SIG_v}(j_\Sigma, j, \theta_\mathrm{v}, \tau_\mathrm{v}) \times \langle u_\mathrm{v}\rangle}{S(j_\Sigma, j) \times \Theta_\mathrm{v}(\theta_\mathrm{v}) \times Q(\mathrm{v}_\Sigma, \mathrm{v}) \times \sigma_{\mathrm{v}\Sigma}\left(\lambda_{MPI,\mathrm{v}}\right) \times \Delta_\mathrm{v}(\tau_\mathrm{v}) \times \Gamma_\mathrm{v} \times f(I_\mathrm{v})} \quad (5)$$

Plugging this result back into Eq. (2) yields the following.

$$P_{0-\mathrm{v}} \cong \frac{N_\mathrm{v}}{N_0} = \frac{\sum_j \frac{\mathrm{SIG_v}(j_\Sigma, j, \theta_\mathrm{v}, \tau_\mathrm{v}) \times \langle u_\mathrm{v}\rangle}{S(j_\Sigma, j) \times \Theta_\mathrm{v}(\theta_\mathrm{v}) \times Q(\mathrm{v}_\Sigma, \mathrm{v}) \times \sigma_{\mathrm{v}\Sigma}\left(\lambda_{MPI,\mathrm{v}}\right) \times \Delta_\mathrm{v}(\tau_\mathrm{v}) \times \Gamma_\mathrm{v} \times f(I_\mathrm{v})}}{\sum_j \frac{\mathrm{SIG_0}(j_\Sigma, j, \theta_0, \tau_0) \times \langle u_0\rangle}{S(j_\Sigma, j) \times \Theta_0(\theta_0) \times Q(\mathrm{v}_\Sigma, 0) \times \sigma_{\mathrm{v}\Sigma}\left(\lambda_{MPI,0}\right) \times \Delta_0(\tau_0) \times \Gamma_0 \times f(I_0)}} \quad (6)$$

This expression can be simplified, since under our experimental conditions the first (resonant) step in the (1+1) REMPI scheme is saturated. Saturation means that the signal is independent of the rotational line strengths, $S(j_\Sigma, j)$, and Franck-Condon factors, $Q(\mathrm{v}_\Sigma, \mathrm{v})$ The saturation of the resonant step in the (1+1) REMPI scheme is discussed in Section 3e in relation to the laser pulse energy dependence. This leads to the key expression used to derive absolute vibrational excitation probabilities:

$$P_{0-\mathrm{v}} \cong \frac{N_\mathrm{v}}{N_0}$$

$$= \left(\frac{\sum_j \mathrm{SIG_v}(j_\Sigma, j, \theta_\mathrm{v}, \tau_\mathrm{v})}{\sum_j \mathrm{SIG_0}(j_\Sigma, j, \theta_0, \tau_0)}\right) \frac{\langle u_\mathrm{v} \rangle \times \Theta_0(\theta_0) \times \sigma_{\mathrm{v}\Sigma}(\lambda_{MPI,0}) \times \Delta_0(\tau_0) \times \Gamma_0 \times f(I_0)}{\langle u_0 \rangle \times \Theta_\mathrm{v}(\theta_\mathrm{v}) \times \sigma_{\mathrm{v}\Sigma}(\lambda_{MPI,\mathrm{v}}) \times \Delta_\mathrm{v}(\tau_\mathrm{v}) \times \Gamma_\mathrm{v} \times f(I_\mathrm{v})} \quad (7)$$

In the following sections, we describe the practical implementation of the above described approach. Briefly, we carry out measurements of $\sum_j SIG_\mathrm{v}(j_\Sigma, j, \theta_\mathrm{v}, \tau_\mathrm{v})$ by conducting laser scans over an entire vibronic band at chosen values of $\theta_\mathrm{v}, \tau_\mathrm{v}, \Gamma_\mathrm{v}$ and I_v and then integrating the signal intensity over the entire band. Rotationally resolved REMPI spectra are recorded via spectrally well isolated bands, which determines $\lambda_{MPI,\mathrm{v}}$. We adjust Γ_v to avoid MCP saturation and I_v to ensure saturation of the resonant step in the REMPI scheme. In separate but similar experiments we measure $\sum_j SIG_0(j_\Sigma, j, \theta_0, \tau_0)$, choosing $\theta_0, \tau_0, \Gamma_0$ and I_0 based on similar considerations. In the absence of trapping and for the case where $N_v \ll N_0$, N_0 is nearly independent of surface temperature, which we verified. Thus for each incidence energy of translation, a single value of N_0 measured at T_S=300K is used to derive $P_{0\text{-}v}$ for different surface temperatures. We also carry out measurements of angular distributions, Θ_v and Θ_0, and time delay distributions, Δ_v and Δ_0, to account for the specific scattering angle and delay time θ_v and τ_v chosen for the measurement of the signal $SIG_\mathrm{v}(j_\Sigma, j, \theta_\mathrm{v}, \tau_\mathrm{v})$. We used literature values of ionization cross-sections

$\sigma_{v_\Sigma}(\lambda_{MPI,v})$35, 36.[35,36] The laser pulse energy dependence of the REMPI signal is measured and fit to a suitable empirical function. We also experimentally characterize the dependence of the signal on the voltage across the MCP detector. With such data in hand, we generate a single value of P_{0-v} at a specific choice of v, incidence energy of translation, E_i, and surface temperature, T_S. This procedure was repeated more than 140 times for different values of E_i, T_S for NO(v=0→1), and NO(v=0→2).

B. Primary observations: REMPI scans of isolated vibronic bands; $\sum_j SIG_v(j_\Sigma, j, \theta_v, \tau_v)$

For each incidence energy listed in Table 1, (1+1) REMPI spectra probing NO(v=0, 1, 2) were recorded at surface temperatures between T_S=300 and 1000 K. Typical REMPI spectra are shown in Fig. 2. The area under the entire REMPI spectrum is obtained by numerical integration providing the spectral intensity, $\sum_j SIG_v(j_\Sigma, j, \theta_v, \tau_v)$, for each vibrational state. Integration over the entire band is advantageous as individual rotational line strength factors and knowledge of the variation of rotational temperature with the surface temperature are not required. At each value of E_i, REMPI spectra such as those of Fig. 2 are measured at several values of T_S. We compare the measurements of the vibrationally excited molecules at various surface temperatures to NO(v=0) spectra taken at T_S = 300K. Comparison to a single measurement helps minimize the random error in the measurement and changes in the scattered NO(v=0) due to surface temperature is minor since the absolute excitation probability does not exceed 6%.

An estimate of the vibrational excitation probability can already be drawn by inspection of the intensity of the REMPI spectra shown in Fig. 2, which have only been corrected for differences in MCP gain and laser pulse energy. These corrections are experimentally measured

and described in more detail in section 3e. We find that the integrated REMPI signal of NO in its ground vibrational state, $\sum_j SIG_0(j_\Sigma, j, \theta_0, \tau_0)$, is ~100-*fold* larger than that of NO(v=1), $\sum_j SIG_1(j_\Sigma, j, \theta_1, \tau_1)$, which is, in turn, ~25-fold larger than that originating from NO(v=2), $\sum_j SIG_2(j_\Sigma, j, \theta_2, \tau_2)$. These numbers agree with the real excitation probabilities within about a factor of two, indicating that the MCP gain and the laser power are the dominant correction factors for quantitative determination of the absolute excitation .

The NO molecules are probed via the γ_{0v} bands, which are well isolated from other bands of the γ-system and REMPI transitions through other intermediate electronic states. The γ_{02} band is a good example of the bands used in this work. Consider that the nearest overlapping band is γ_{13}, which probes NO(v=3). Overlapping lines from this band are much weaker as NO(v=3) is much less populated than NO(v=2)[37]. This is demonstrated in Fig. 3. Note that all of the observed lines can be assigned to the γ_{02} band, even those in the inset, where the band-head of γ_{13} is found. This shows that spectral overlap with other bands is avoided and a simple integration over the entire REMPI spectrum yields, in this case, $\sum_j SIG_2(j_\Sigma, j, \theta_2, \tau_2)$. For NO(v=0→1), a small background was observed which arises from rotationally inelastic, vibrationally elastic scattering of thermally populated NO(v=1) present in the incident molecular beam. This small contribution to the signal was determined by extrapolating the surface temperature dependence of the NO(v=1) signal to T_s=0 K using a suitable Arrhenius expression, and then subtracted.

The rotationally resolved REMPI spectra recorded in the course of absolute excitation probability measurements carry much more information than just the integrated signal. These rotational spectra, examples of which are shown in Fig. 2, have been fit, using LIFBase[38], to extract a rotational temperature which characterizes the rotational population distributions.

Derived rotational temperatures as a function of surface temperature and incidence energy are shown in Fig. 4. While there is no reason to expect a thermal rotational distribution, the rotational excitation is well approximated by a thermal distribution, a rotational temperature allows and thus a simple and sensible way to compare the extent of rotational excitation of the molecules upon scattering from the surface.

The rotational temperature of the scattered molecules does not depend strongly on the final vibrational state. The rotational excitation increases when surface temperature or incidence energy is increased. The rotational temperature, except by coincidence, is different than the temperature of the surface, indicating a direct scattering mechanism. These trends in rotational excitation are qualitatively similar to NO scattering from Ag(111).[11]

C. Primary observations: angular distributions; $\Theta_v(\theta_v)$

The angular distributions of scattered molecules are, in principle, dependent upon T_S, E_i and v. Broader angular distributions result in smaller REMPI signals for the same amount of scattered molecules due to spatial dilution. The (1+1) REMPI used in this work employs an unfocused laser, meaning the detection volume is cylindrical with the long axis along the laser propagation direction. This implies that the flux of molecules is linearly proportional to the measured angular distribution, $\Theta_v(\theta_v)$. For narrow angular distributions characteristic of direct scattering, the difference in the resulting signals obtained using a point or a cylindrical detection volume is small. However as the angular distribution broadens, the difference becomes larger. For example, for the case of the molecules departing the surface by thermal desorption, which exhibits a cosθ angular distribution, the angular distribution recorded along the cylindrical detection region appears with a $\cos^2\theta$ dependence, since the measured signal is proportional to the scattered molecular density integrated along the line of sight of the REMPI laser.

Angular distributions of the scattered vibrationally excited molecules were measured for each incidence translational energy described in the experimental section for at least three surface temperatures. These were measured by tuning the laser wavelength to a single REMPI transition and linearly translating the laser parallel to the surface. While ideally the measurement of angular distributions would be measured in a circular arc around the scattering center, for narrow angular distributions the deviations between angular distributions by translating the laser in a circular arc and those measured by translating the laser beam parallel to the surface are negligible. Hence, in this work the correction for these deviations was not required, especially in the view of the fact that scattered angular distributions did not vary significantly for different experimental conditions. For convenience Θ_0 was measured at T_S=300K. REMPI spectra of scattered molecules were typically recorded off the peak of the angular distribution to avoid the spatial overlap of the probe laser with the incident (nearly normal to the surface) molecular beam. The angular distributions observed for NO/Au(111) system, although narrow, are generally broader than those previously measured for the HCl/Au(111) system using a similar experimental setup.[39] For HCl, translational energy couples strongly to vibration.[8,32] The scattered vibrationally excited molecules only have enough translational energy to escape the surface at scattering angles near the surface normal. However for NO the translation to vibration coupling is very weak[40] allowing for a broader final angular distribution of scattered molecules.

The angular distributions peak at the specular angle and are much narrower than a $\cos^2\theta$ distribution, which would characterize the molecules undergoing trapping desorption with no dependence of the trapping probability on incidence angle. This result is consistent with the rotational temperature dependencies described above, also indicating direct sub-ps single bounce scattering dynamics.

Each measured angular distribution was fitted to a normalized Gaussian function.

$$\Theta_v(\theta) = \frac{e^{-\frac{1}{2}\left(\frac{\theta-\theta_0}{\sigma}\right)^2}}{\sqrt{2\pi}\,\sigma} \qquad (8)$$

Here, θ_0 is the scattering angle of peak intensity and σ is the width parameter of the angular distribution related to the full width at half maximum ($FWHM = 2\sigma\sqrt{2\ln 2}$). Values of σ determined from these fits are given in Appendix A. We used linear interpolation of the width parameter, σ, to characterize angular distributions at temperatures where measurements were not carried out, since the measured Θ_v's vary only slightly within the range of temperatures used in this work, as shown in Fig. 5. Figure 6 shows the variation in the width parameters with incidence energy. Data is shown for scattered v=0 and T_S=300K and for v=1 and v=2 at T_S=1000K. The width decreases slightly with increasing E_i. The width of the distribution increases slightly with increasing surface temperature as shown in Fig. 5 and Appendix A.

D. Primary observations: delay time profiles; $\Delta_v(\tau)$

The delay time profiles, $\Delta_v(\tau)$, are utilized in a similar way as the angular distributions. ddelay time profiles and for differences in the specific value of τ_v at which the experiment was conducted. The delay scan profiles, $\Delta_v(\tau)$, depend very weakly on the final vibrational state, as shown in the left panel of Fig. 7. There is a surface temperature influence, albeit also weak, on $\Delta_v(\tau)$, shown in the right panel of Fig. 7 for $\Delta_1(\tau)$.

E. Primary observations: laser pulse energy dependence, A-state ionization cross sections and MCP gain

The magnitude of the REMPI signals depends strongly on the laser pulse energy, which is taken into account by normalizing the recorded REMPI signal with an empirical function, $f(I_v)$, derived by fitting the measured power dependence. At low pulse energies neither step of the two-photon absorption process is saturated, resulting in a quadratic dependence of the REMPI signal on the laser pulse energy. At intermediate energies the resonant first photon absorption becomes saturated[41-43], leading to a linear laser pulse energy dependence. At sufficiently high pulse energies both absorption steps become saturated, resulting in laser-power independent REMPI signal.

$$f(I_v) \propto \begin{cases} {I_v}^2 & \text{(at low pulse energy)} \\ I_v & \text{(at intermediate pulse energy)} \\ \text{constant} & \text{(at high pulse energy)} \end{cases} \qquad (9)$$

For (1+1) REMPI used in this work, the laser was unfocused with a width of 2 mm, we observe a quadratic dependence below a pulse energy of 0.4 mJ, which becomes linear above ~1 mJ.

We do not observe the two-photon saturated behavior under our conditions. The reason for this becomes apparent when employing a two-color (1+1′) REMPI approach. Here, a 2 mm diameter beam of ~230 nm light from the doubled output of the tunable dye laser, with a pulse energy between 0.1 and 2 mJ was tuned onto a resonance of the γ-band and was coaxially overlapped with a 2 mm beam of the Nd:YAG laser's 4th harmonic at 266 nm with a constant pulse energy of 24mJ. Under these conditions, NO is resonantly excited to the $A^2\Sigma^+$ state by the output of the low intensity pulse at ~230 nm and the $A^2\Sigma^+$ state is ionized by both the 230 nm and 266 nm light. Since the ionization cross sections for 230 nm and 266 nm are thought to be similar[43], the ionization is dominated by the more intense 266 nm pulse and approximately independent of the intensity of the ~230 nm light. Figure 8 shows the dependence of this (1+1′)

signal on the energy of the 230 nm pulse for the γ_{01} band. One can clearly see the saturation of the resonant step of the γ band at a pulse energy of about 1 mJ. In contrast, even with 24 mJ/pulse at 266 nm, the ionization step is not saturated.

For one-color REMPI, laser pulse energy dependencies, $f(I_v)$, were measured for different bands probing scattered NO(v=0, 1 and 2) as well as NO(v=0) prepared by leaking NO into the chamber. The results of these measurements, Fig. 9, are interesting to compare to those of Fig. 8. As expected one sees a quadratic intensity dependence at the lowest energies which becomes linear above a laser pulse energy of 1 mJ showing that the second step is not saturated. We find that the laser intensity dependence can be approximated reasonably well by an empirical function $f(\mathrm{I_v}) \propto \mathrm{I_v}^{1.66}$ over the entire laser intensity range used in this work, independent of vibrational state. This empirical function was used to normalize observed signals to the laser pulse energy. Note that the ionization efficiency is nearly identical when probing different vibrational states since the ionization cross section of the $A^2\Sigma^+$ state is only weakly wavelength dependent between λ_{MPI}=225 and 324nm[35,36,41] and all vibrational states are excited to the $A^2\Sigma^+$ (v_Σ=0) state prior to the ionization step. Furthermore, one-color (1+1) REMPI was always used with laser pulse energies substantially above 1 mJ, ensuring saturation of the resonant transition in the γ-band. Thus the (1+1) REMPI signal originating from different vibrational states is independent of the Franck-Condon factors $Q(\mathrm{v_\Sigma}, \mathrm{v})$ of the corresponding vibronic transitions.

The gain of the MCP, Γ_v, varies as the voltage across the MCP is adjusted to optimize conditions for the detection of each vibrational state. The gain of the MCP is set to a value that allows for a satisfactory signal to noise ratio while avoiding saturation of the MCP. The gain

factor, Γ_v, was experimentally measured over a wide range of voltages, V, and is given as follows.

$$\Gamma \propto V^{17.8\pm0.45} \qquad (10)$$

Eq. 10 was valid for $1200\text{V} < V < 2000\text{V}$.

F. The density-to-flux conversion

As previously mentioned, knowledge of final velocity of the scattered molecules, $\langle u_v \rangle$, is used to convert the REMPI derived density measurement to flux, which is proportional to the state-to-state scattering probability. These velocities were derived from IR-UV double resonance TOF measurements in a fashion similar to previous work[32,33]. The translational inelasticity, $\langle \frac{1/2\, m\, u_{\text{scattered}}{}^2}{1/2\, m\, u_{\text{incident}}{}^2} \rangle$, for the vibrationally elastic scattering channel, NO (v=0→0), was found to be ~0.5. For vibrationally inelastic channels, NO (v=0→1,2), an additional translational energy loss was seen, corresponding to ~ 8% of the vibrational excitation energy gained by the molecule. A comprehensive report of T-V coupling during the course of vibrational excitation and relaxation of NO upon scattering from Au(111) is forthcoming.

Since the final translational energy is approximately independent of vibrational state, the density-to-flux conversion correction factor is negligible under nearly all of our conditions. An important exception is the lowest incidence translational energy of this work, E_i=0.11 eV. Here the correction is significant since any T-V coupling represents a larger fraction of the translational energy.

4. DISCUSSION

The derived vibrational excitation probabilities for NO(v=0→1) and NO(v=0→2) are shown in Fig. 10 and listed in Appendix B. The error bars on the experimental data were determined by estimating the statistical uncertainties in all input variables and then calculating their propagation into the absolute excitation probability, see Appendix C.

The input variables and their estimated relative uncertainties are the integrated signal intensities, $SIG_v(j,j_\Sigma,\theta_v,\tau_v)$ (1%), the mean velocities, $\langle u_v \rangle$ (5%), the angular dilution corrections, $\Theta_v(\theta_0)$ (5%), the temporal dilution corrections, $\Delta_v(\tau_v)$ (5%), the MCP voltages, U_v (0.5%), and the mean laser pulse energies I_v (20%). Note that in the equation (7), which represents the derived excitation probabilities in terms of these quantities, all of these variables appear for v=0 and for v=1,2,3, that is in the numerator and in the denominator.

The propagation of experimental uncertainties Δx_i into the excitation probability P was calculated according to $\Delta P = \sqrt{\sum \left(\frac{\partial P}{\partial x_i}\Delta x_i\right)^2}$. As P is of the form $P = \prod_i {x_i}^{n_i}$, the relative uncertainty may be expressed as a function of the relative uncertainties of the input variables as $\Delta P/P = \sqrt{\sum (n_i\, \Delta x_i/x_i)^2}$, where the exponents n_i are ±1 except for U_v (n=17.8) and I_v (n=1.66).

For the given estimated uncertainties on the input parameters, we find that $\Delta P/P$ ~ 50%. These uncertainties are listed in Appendix B. The largest contributions originate from fluctuations in the laser pulse energy.

At all incidence energies, the vibrational excitation probabilities follow an Arrhenius dependence on surface temperature (solid lines) with an activation-energy equal to the change of the vibrational energy. This is true for both the single and double-quantum vibrational excitation.

This Arrhenius surface temperature dependence is commonly attributed to the distribution of thermally excited EHPs which mediate vibrational excitation[7-9,12,13].

In all cases the vibrational excitation is at least one order of magnitude higher for NO(v=0→1) than for NO(v=0→2). The population ratio between the two excited vibrational states is nearly independent of incidence energy. The fact that the vibrational excitation exhibits an Arrhenius surface temperature dependence at all incidence energies, with the activation energy equal to the vibrational spacing as well as that the relative excitation NO(v=0→1) to that of NO(v=0→2) is independent of incident energy indicates that over the wide translational energy and surface temperature range used in this study the predominant mechanism for vibrational excitation of NO scattering from Au(111) is electronically non-adiabatic coupling.

The solid lines of Fig. 10 demonstrate that the excitation probabilities follow an Arrhenius dependence on surface temperature and from this an Arrhenius pre-exponential factor can be obtained. The Arrhenius pre-factors are plotted vs. E_i in Fig. 11. Error bars representing 90% confidence intervals were calculated according to the Student's t-test. Due to background issues stemming from NO(v=1) native in the incident beam (see above) excitation probabilities measured at T_S=300K have been neglected from the Arrhenius pre-factor comparison.

The Arrhenius pre-factors are useful as they indicate the intrinsic strength of the nonadiabatic coupling that induces vibrational excitation, decoupling it from the factors that only reflect the EHP thermal population distribution[7]. They are limited to values between 0 and 1. An upper value of 1 indicates that the coupling is strong enough to allow full equilibration between vibration and the EHP bath on the time scale of the collision. The values obtained in this work, ranging from 0.17 to 0.85, represent strong coupling between the molecular vibration and the

EHP bath of the metal, for example in comparison to vibrational excitation of HCl(v=0→1) when scattered from Au(111),[1,8] where pre-factors of 0.002 were derived. Consistent with earlier observations, there is a strong incidence energy dependence in nonadiabatic vibrational excitation[10,12]. At the highest incidence energies the excitation probabilities approach those expected for thermal equilibrium with the surface.

At most incidence translational energies the ratio between the Arrhenius pre-factors for NO(v=0→2) and NO(v=0→1) is near 0.8. The similar magnitude of the pre-exponential factors for NO(v=0→1) and for NO(v=0→2) vibrational excitation hints at the mechanism of direct overtone vibrational excitation[7,9]. Should v=2 be populated by a sequential mechanism – NO(v=0→1→2) – the pre-exponential factor for Δv=2 would be on the order of the square of that for Δv=1, however as seen in Fig. 11 the pre-exponential is roughly the same for both NO(v=0→2) and NO(v=0→1). The similarity in magnitude between single and overtone excitation pre-exponential factors indicates that NO(v=0→2) excitation occurs primarily via direct overtone transition.

One interesting implication of our results, which can be seen in Fig. 11, concerns the extrapolation to E_i=0. The results seem to suggest that the intrinsic excitation probability does not vanish at zero incidence energy of translation. This might be evidence for a steering effect, since theory shows that when NO approaches Au(111) nitrogen atom first, electronically nonadiabatic coupling is enhanced[21]. However, this implication should be considered carefully. At low incidence energies of translation, the density-to-flux correction described above islarge. Any errors in its evaluation might alter the results at the lowest values of E_i enough to change this qualitative conclusion. Improved experiments that might resolve this uncertainty are currently underway.

In addition, if trapping desorption were to play an important role, it might alter the interpretation of these observations especially at the lowest values of E_i used in this work. The trapping probability of NO scattering on Au(111) has been previously measured[44] and IESH dynamical calculations[19] using a potential surface derived from DFT[20] give reasonable agreement with these measurements. The well depth of this DFT derived potential surface is 0.13 eV. We can estimate the residence time of trapped NO on the Au(111) surface using statistical models[44] and these show that, not surprisingly, the residence time in this case can be substantially longer (1-10 ps time scale) than the interaction time in direct scattering. Of course, the increased residence time might allow for more probable vibrational excitation.

The angular distributions (see Fig.'s 6 and 12) for both NO(v=0→1) and NO(v=0→2) scattering channels at E_i=0.11 eV are broader than those seen at higher incidence energies, an observation that might suggest trapping desorption is playing a role here. This alone does not indicate that trapping desorption is the predominant mechanism because as the incidence kinetic energy is lowered, the energy of a hot surface (1000K corresponds to ~0.09eV) becomes comparable to the incident translational energy which could lead to a dramatic broadening of the scattered angular distribution. However the fact that the angular distribution at E_i=0.11 eV, $\cos(\theta)^{2.5}$, is virtually indistinguishable from the expectation of trapping desorption, $\cos(\theta)^2$, is strong proof that at the lowest incidence energy trapping desorption is the predominant mechanism.

5. CONCLUSIONS

We have provided a comprehensive description of the method for deriving absolute vibrational excitation probabilities from molecular beam surface scattering experiments. The

experimental aspects concerning spectral, angular and temporal distributions as well as influence of laser pulse energy on the derived absolute vibrational excitation probabilities were presented and discussed in detail. Arrhenius pre-factors, a measure of the strength of the vibration electron coupling, were extracted from the vibrational excitation probabilities and these showed a strong dependence on the incidence energy. The coupling between vibration of the molecule and EHPs of the metal is strong enough at higher incidence energies to allow approach to the thermal limit of vibrational excitation both for NO(v=0→1) and NO(v=0→2) channels. The similar magnitudes of the Arrhenius pre-factors for single and double-quantum vibrational excitation suggests that NO(v=0→2) excitation occurs predominantly via direct overtone excitation. In addition to quantitative evaluation of absolute vibrational excitation probabilities, the rotational distributions and angular distributions provide an important handle to study the scattering dynamics in the NO/Au(111) system. The described experimental approach generates an extensive set of data to which theoretical models of electronically nonadiabatic phenomena can be compared.

6. ACKNOWLEDGEMENTS

CB, DJA, and AMW acknowledge support from the Alexander von Humboldt foundation.

[1]I. Rahinov, R. Cooper, D. Matsiev, C. Bartels, D. J. Auerbach, and A. M. Wodtke, PCCP **13** (28), 12680 (2011).
[2]C. Bartels, R. Cooper, D. J. Auerbach, and A. M. Wodtke, Chem. Sci. **2** (9), 1647 (2011).
[3]A. M. Wodtke, J. C. Tully, and D. J. Auerbach, Int. Rev. Phys. Chem. **23** (4), 513 (2004).
[4]Y. Huang, C. T. Rettner, D. J. Auerbach, and A. M. Wodtke, Science **290** (5489), 111 (2000).
[5]J. D. White, J. Chen, D. Matsiev, D. J. Auerbach, and A. M. Wodtke, Nature **433** (7025), 503 (2005).
[6]N. H. Nahler, J. D. White, J. LaRue, D. J. Auerbach, and A. M. Wodtke, Science **321** (5893), 1191 (2008).
[7]D. Matsiev, Z. Li, R. Cooper, I. Rahinov, C. Bartels, D. J. Auerbach, and A. M. Wodtke, PCCP **13** (18), 8153 (2011).
[8]Q. Ran, D. Matsiev, D. J. Auerbach, and A. M. Wodtke, Phys. Rev. Lett. **98** (23) (2007).

[9]R. Cooper, I. Rahinov, Z. Li, D. Matsiev, D. J. Auerbach, and A. M. Wodtke, Chem. Sci. (1), 55 (2010).
[10]C. T. Rettner, J. Kimman, F. Fabre, D. J. Auerbach, and H. Morawitz, Surf. Sci. **192** (1), 107 (1987).
[11]C. T. Rettner, J. Kimman, and D. J. Auerbach, J. Chem. Phys. **94** (1), 734 (1991).
[12]C. T. Rettner, F. Fabre, J. Kimman, and D. J. Auerbach, Phys. Rev. Lett. **55** (18), 1904 (1985).
[13]E. K. Watts, J. L. W. Siders, and G. O. Sitz, Surf. Sci. **374** (1-3), 191 (1997).
[14]J. C. Tully, Annu. Rev. Phys. Chem. **51** (1), 153 (2000).
[15]Y. J. Chabal, Phys. Rev. Lett. **55** (8), 845 (1985).
[16]M. Morin, N. J. Levinos, and A. L. Harris, J. Chem. Phys. **96** (5), 3950 (1992).
[17]E. Hasselbrink, Curr. Op. Solid St. Mat. Sci. **10** (3-4), 192 (2006).
[18]E. Hasselbrink, Surf. Sci. **603** (10-12), 1564 (2009).
[19]N. Shenvi, S. Roy, and J. C. Tully, J. Chem. Phys. **130** (17), 174107 (2009).
[20]S. Roy, N. A. Shenvi, and J. C. Tully, J. Chem. Phys. **130** (17), 174716 (2009).
[21]N. Shenvi, S. Roy, and J. C. Tully, Science **326** (5954), 829 (2009).
[22]M. Head-Gordon and J. C. Tully, *Molecular dynamics with electronic frictions*. **103** (23), 10137. (AIP, 1995).
[23]M. Head-Gordon and J. C. Tully, *Vibrational relaxation on metal surfaces: Molecular-orbital theory and application to CO/Cu(100)*. **96** (5), 3939. (AIP, 1992).
[24]S. Monturet and P. Saalfrank, Phys. Rev. B **82** (7), 075404 (2010).
[25]J. W. Gadzuk, J. Chem. Phys. **79** (12), 6341 (1983).
[26]D. M. Newns, Surf. Sci. **171** (3), 600 (1986).
[27]B. N. J. Persson and M. Persson, Solid State Commun. **36** (2), 175 (1980).
[28]Y. Huang, A. M. Wodtke, H. Hou, C. T. Rettner, and D. J. Auerbach, Phys. Rev. Lett. **84** (13), 2985 (2000).
[29]J. LaRue, T. Schafer, D. Matsiev, L. Velarde, N. H. Nahler, D. J. Auerbach, and A. M. Wodtke, PCCP (2011).
[30]R. Cooper, C. Bartels, A. Kandratsenka, I. Rahinov, N. Shenvi, K. Golibrzuch, Z. Li, D. J. Auerbach, J. C. Tully, and A. M. Wodtke, Angew. Chem., DOI: 10.1002/anie.201201168 (2012).
[31]Q. Ran, D. Matsiev, A. M. Wodtke, and D. J. Auerbach, Rev. Sci. Instrum. **78** (10), 104104 (2007).
[32]I. Rahinov, R. Cooper, C. Yuan, X. Yang, D. J. Auerbach, and A. M. Wodtke, J. Chem. Phys. **129** (21), 214708 (2008).
[33]R. Cooper, I. Rahinov, C. Yuan, X. Yang, D. J. Auerbach, and A. M. Wodtke, J. Vac. Sci. Technol., A **27** (4), 907 (2009).
[34]In principle a more precise treatment for the density-to-flux conversion would utilize the full velocity distribution. In practice under the experimental conditions used here this is not nescasary as the denisty-to-flux converstion is rather small. Experimentalists treating other systems with this or other exxperimetnal methods should pay strict attention to the approximation used in this work and whether it still holds in other cases.
[35]S. N. Dixit, D. L. Lynch, V. McKoy, and W. M. Huo, Phys. Rev. A **32** (2), 1267 (1985).
[36]H. Rudolph, S. N. Dixit, V. McKoy, and W. M. Huo, J. Chem. Phys. **88** (2), 637 (1988).
[37]Preliminary results show that NO(v=3) is at least a factor of 10 less populated than NO(v=2) under the experimental conditions used in this work.
[38]J. Luque, Crosley, D.R. , LIFBASE: Database and Spectral Simulation Program (1999).

[39]Q. Ran, D. Matsiev, D. J. Auerbach, and A. M. Wodtke, Nuclear Instruments & Methods in Physics Research Section B-Beam Interactions with Materials and Atoms **258** (1), 1 (2007).
[40]To be published.
[41]H. Zacharias, F. d. Rougemont, T. F. Heinz, and M. M. T. Loy, J. Chem. Phys. **105** (1), 111 (1996).
[42]D. C. Jacobs, R. J. Madix, and R. N. Zare, J. Chem. Phys. **85** (10), 5469 (1986).
[43]M. Hippler and J. Pfab, Chem. Phys. Lett. **243** (5-6), 500 (1995).
[44]A. M. Wodtke, H. Yuhui, and D. J. Auerbach, Chem. Phys. Lett. **413** (4-6), 326 (2005).

7. Appedices

A. Angular distribuiton width parameteres

Incidence Energy (E_i/eV)	Surface Temperature (T_S/K)	Angular width parameter ($\sigma/°$)[a]
NO(v=0→0)		
0.11	303	20
0.28	303	18
0.41	912	16
0.41	310	17
0.41	303	18
0.63	303	17
0.93	946	16
0.93	652	15
0.93	308	17
0.93	303	18
0.93	303	19
0.93	303	18
1.05	303	18
NO(v=0→1)		
0.11	973	22
0.11	633	23
0.11	323	19
0.28	973	22
0.28	633	20
0.28	323	19
0.41	943	18
0.41	543	18
0.63	973	20
0.63	633	16
0.63	353	15
0.93	983	18
0.93	980	18
0.93	660	17
0.93	330	16
1.05	973	17
1.05	973	18
1.05	763	17
1.05	753	16
1.05	333	15
1.05	318	15
NO(v=0→2)		
0.11	973	25
0.28	973	22
0.28	848	21

0.41	998	18
0.41	703	19
0.63	973	19
0.63	823	18
0.63	683	17
0.93	983	18
0.93	962	19
0.93	923	20
0.93	791	17
0.93	774	16
1.05	972	18
1.05	846	18
1.05	637	17

[a]These parameters refer to Eq. 8.

B. Absolute vibrational excitation probabilities

Incidence Energy (E_i/eV)	Surface Temperature (T_S/K)	Excitation Probability	Error
NO(v=0→1)			
0.11	973	1.1×10^{-02}	5.5×10^{-03}
0.11	873	8.0×10^{-03}	4.0×10^{-03}
0.11	753	4.0×10^{-03}	2.0×10^{-03}
0.11	633	2.0×10^{-03}	1.0×10^{-03}
0.11	503	7.0×10^{-04}	3.5×10^{-04}
0.28	973	1.2×10^{-02}	6.0×10^{-03}
0.28	873	8.0×10^{-03}	4.0×10^{-03}
0.28	753	7.0×10^{-03}	3.5×10^{-03}
0.28	633	3.0×10^{-03}	1.5×10^{-03}
0.28	493	1.2×10^{-03}	6.0×10^{-04}
0.28	323	2.0×10^{-04}	1.0×10^{-04}
0.41	1073	3.0×10^{-02}	1.5×10^{-02}
0.41	973	2.0×10^{-02}	1.0×10^{-02}
0.41	878	1.6×10^{-02}	8.0×10^{-03}
0.41	776	1.1×10^{-02}	5.5×10^{-03}
0.41	673	6.0×10^{-03}	3.0×10^{-03}
0.41	673	7.0×10^{-03}	3.5×10^{-03}
0.41	573	2.0×10^{-03}	1.0×10^{-03}
0.41	573	2.0×10^{-03}	1.0×10^{-03}
0.41	473	2.0×10^{-03}	1.0×10^{-03}
0.41	473	2.0×10^{-03}	1.0×10^{-03}
0.41	373	7.0×10^{-04}	3.5×10^{-04}
0.41	373	6.0×10^{-04}	3.0×10^{-04}
0.63	973	1.9×10^{-02}	9.5×10^{-03}
0.63	873	1.3×10^{-02}	6.5×10^{-03}
0.63	753	8.0×10^{-03}	4.0×10^{-03}
0.63	633	4.0×10^{-03}	2.0×10^{-03}
0.63	493	9.0×10^{-04}	4.5×10^{-04}
0.93	988	3.2×10^{-02}	1.6×10^{-02}
0.93	951	3.5×10^{-02}	1.8×10^{-02}
0.93	893	2.2×10^{-02}	1.1×10^{-02}
0.93	813	1.7×10^{-02}	8.5×10^{-03}
0.93	768	1.6×10^{-02}	8.0×10^{-03}
0.93	728	1.4×10^{-02}	7.0×10^{-03}
0.93	698	1.7×10^{-02}	8.5×10^{-03}
0.93	660	1.1×10^{-02}	5.5×10^{-03}
0.93	643	8.0×10^{-03}	4.0×10^{-03}
0.93	598	8.0×10^{-03}	4.0×10^{-03}
0.93	568	4.0×10^{-03}	2.0×10^{-03}
0.93	473	5.0×10^{-03}	2.5×10^{-03}
0.93	436	1.0×10^{-03}	5.0×10^{-04}

0.93	378	2.0×10^{-03}	1.0×10^{-03}
0.93	338	5.0×10^{-04}	2.5×10^{-04}
1.05	973	5.3×10^{-02}	2.7×10^{-02}
1.05	873	3.5×10^{-02}	1.8×10^{-02}
1.05	763	1.7×10^{-02}	8.5×10^{-03}
1.05	633	9.0×10^{-03}	4.5×10^{-03}
1.05	493	3.0×10^{-03}	1.5×10^{-03}
NO(v=0→2)			
0.11	973	7.3×10^{-04}	3.7×10^{-04}
0.11	918	4.8×10^{-04}	2.4×10^{-04}
0.11	848	2.8×10^{-04}	1.4×10^{-04}
0.11	798	1.4×10^{-04}	7.0×10^{-05}
0.28	973	3.9×10^{-04}	2.0×10^{-04}
0.28	918	2.7×10^{-04}	1.4×10^{-04}
0.28	848	1.6×10^{-04}	8.0×10^{-05}
0.28	788	1.0×10^{-04}	5.0×10^{-05}
0.28	733	7.0×10^{-05}	3.5×10^{-05}
0.41	973	8.2×10^{-04}	4.1×10^{-04}
0.41	948	8.2 x10-04	4.1×10^{-04}
0.41	923	5.9×10^{-04}	3.0×10^{-04}
0.41	873	5.0×10^{-04}	2.5×10^{-04}
0.41	848	3.3×10^{-04}	1.7×10^{-04}
0.41	803	2.2×10^{-04}	1.1×10^{-04}
0.41	746	1.7×10^{-04}	8.5×10^{-05}
0.41	698	8.0×10^{-05}	4.0×10^{-05}
0.41	676	1.3×10^{-04}	6.5×10^{-05}
0.41	973	8.2×10^{-04}	4.1×10^{-04}
0.41	948	8.2×10^{-04}	4.1×10^{-04}
0.41	923	5.9×10^{-04}	3.0×10^{-04}
0.41	873	5.0×10^{-04}	2.5×10^{-04}
0.41	848	3.3×10^{-04}	1.7×10^{-04}
0.41	803	2.2×10^{-04}	1.1×10^{-04}
0.41	746	1.7×10^{-04}	8.5×10^{-05}
0.41	698	8.0×10^{-05}	4.0×10^{-05}
0.41	676	1.3×10^{-04}	6.5×10^{-05}
0.63	973	7.8×10^{-04}	3.9×10^{-04}
0.63	893	4.5×10^{-04}	2.3×10^{-04}
0.63	823	4.4×10^{-04}	2.2×10^{-04}
0.63	753	2.5×10^{-04}	1.3×10^{-04}
0.63	683	1.1×10^{-04}	5.5×10^{-05}
0.63	613	3.0×10^{-05}	1.5×10^{-05}
0.93	983	2.0×10^{-03}	1.0×10^{-03}
0.93	938	1.2×10^{-03}	6.0×10^{-04}
0.93	893	9.2×10^{-04}	4.6×10^{-04}

0.93	850	4.3×10^{-04}	2.2×10^{-04}
0.93	813	4.4×10^{-04}	2.2×10^{-04}
0.93	798	3.4×10^{-04}	1.7×10^{-04}
0.93	776	2.8×10^{-04}	1.4×10^{-04}
0.93	727	2.5×10^{-04}	1.3×10^{-04}
0.93	681	1.6×10^{-04}	8.0×10^{-05}
1.05	973	2.9×10^{-03}	1.5×10^{-03}
1.05	908	1.8×10^{-03}	9.0×10^{-04}
1.05	843	9.0×10^{-04}	4.5×10^{-04}
1.05	813	8.3×10^{-04}	4.2×10^{-04}
1.05	773	4.2×10^{-04}	2.1×10^{-04}
1.05	708	2.9×10^{-04}	1.5×10^{-04}
1.05	583	1.2×10^{-04}	6.0×10^{-05}

C. *Propagation of errors*

The input variables and their estimated relative uncertainties are the integrated signal intensities, $SIG_v(j,j_\Sigma,\theta_v,\tau_v)$ (1%), the mean velocities, $\langle u_v \rangle$ (5%), the angular dilution corrections, $\Theta_v(\theta_0)$ (5%), the temporal dilution corrections, $\Delta_v(\tau_v)$ (5%), the MCP voltages, U_v (0.5%), and the mean laser pulse energies I_v (20%). Note that in the equation (7), which represents the derived excitation probabilities in terms of these quantities, all of these variables appear for v=0 and for v=1,2,3, that is in the numerator and in the denominator.

The propagation of experimental uncertainties Δx_i into the excitation probability P was calculated according to $\Delta P = \sqrt{\sum \left(\frac{\partial P}{\partial x_i}\Delta x_i\right)^2}$. As P is of the form $P = \prod_i {x_i}^{n_i}$, the relative uncertainty may be expressed as a function of the relative uncertainties of the input variables as $\Delta P/P = \sqrt{\sum (n_i\, \Delta x_i/x_i)^2}$, where the exponents n_i are ±1 except for U_v (n=17.8) and I_v (n=1.66).

For the given estimated uncertainties on the input parameters, we find that $\Delta P/P \sim 50\%$. These uncertainties are listed in Appendix B. The largest contributions originate from fluctuations in the laser pulse energy.

8. Tables

Table 1: Incident beam parameters.

Mixing Ratios	$\langle E_i \rangle$, eV	$\sqrt{\left\langle E_i^2 \right\rangle - \langle E_i \rangle^2}$, eV	ν_0, m/s[a]	α, m/s[a]
1%NO/99%H_2	1.05	0.110	2574	195
2.5%NO/97.5%H_2	0.93	0.071	2431	133
6.5% NO/93.5%H_2	0.63	0.084	1973	191
10%NO/90%H_2	0.41	0.049	1611	114
5%NO/25%N_2/70%H_2	0.28	0.041	1305	140
7.5% NO/92.5% N_2	0.11	0.012	818	69

[a] *Experimentally derived parameters which describe the flux distribution function,* $F(v) = Av^3 e^{-\left(\frac{v-v_0}{\alpha}\right)^2}$, *of the beams used in this work.*

Table 2: Definitions of variables and functions

Symbol	Definitions
$\mathrm{SIG_v}(j_\Sigma, j, \theta_\mathrm{v}, \tau_\mathrm{v})$	REMPI signal strength
j	Rotational state of probed molecules
j_Σ	Rotational state of the intermediate state
θ_v	Scattering angle
τ_v	Time delay between pulsed valve and laser
$\mathrm{n_v}(j)$	Rotational population
$\langle u_\mathrm{v} \rangle$,	Average velocity
$S(j_\Sigma, j)$	Rotational line strength factors
$\Theta_\mathrm{v}(\theta)$	Scattering angular distributions function
$Q(\mathrm{v}_\Sigma, \mathrm{v})$	Frank Condon factor
$\sigma_{\mathrm{v}_\Sigma}(\lambda_{MPI,\mathrm{v}})$	Cross section of the intermediate state
$\lambda_{MPI,\mathrm{v}}$	Laser wavelength
$\Delta_\mathrm{v}(\tau)$	Time delay function between pulsed valve and laser
Γ_v	Function of MCP gain
$f(\mathrm{I_v})$	Function of laser pulse energy

9. Figures and Captions

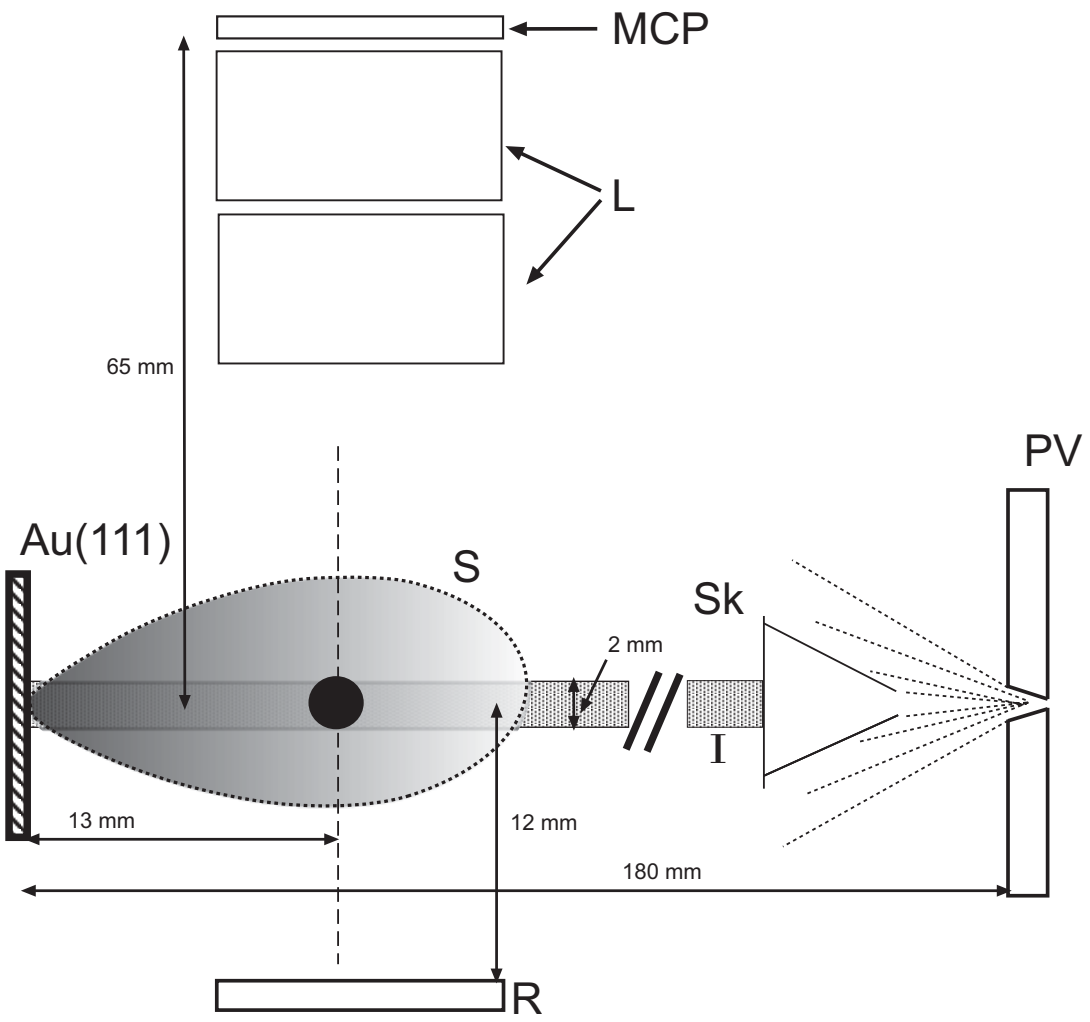

<u>Figure 1: Schematic of the experimental apparatus.</u> The molecules leave the pulsed valve (PV) and pass through a skimmer (Sk). The incident molecular beam (I) strikes a Au(111) surface at nearly normal incidence. The scattered molecules (S) are ionized with a laser (black circle). The ions are directed via a repeller (R) and an ion lens (L) to a microchannel (MCP) plate array where they are detected. The detection laser can be translated parallel to the surface (~22 mm) as represented by the thin dashed line.

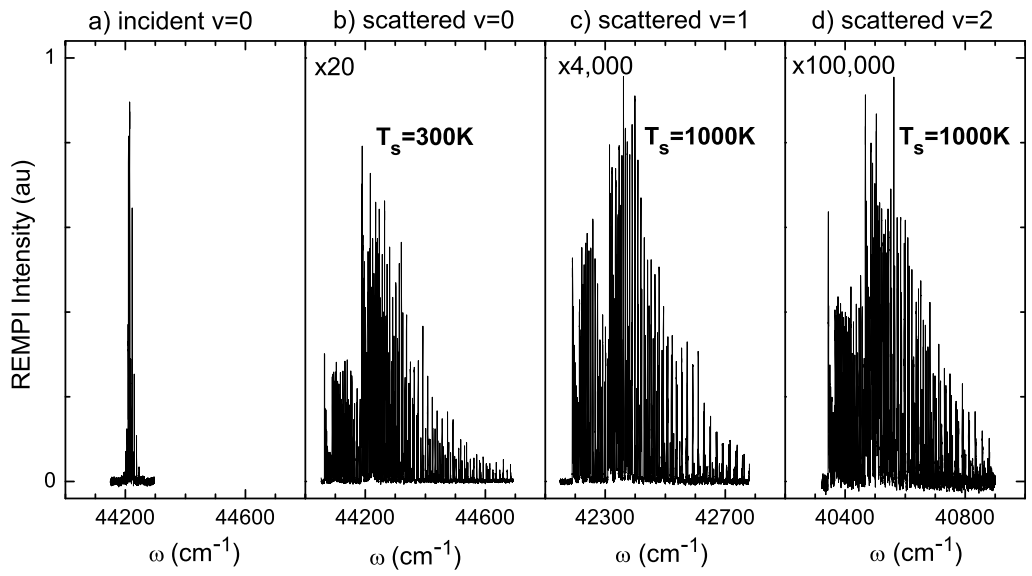

Figure 2: Illustrative REMPI spectra of NO before and after scattering from Au(111) at E_i=0.63eV. a) NO(v=0) probed via the γ_{00} band prior to collision with the surface. b) Scattered NO(v=0) probed via the γ_{00} band. c) Scattered NO(v=1) probed via the γ_{01} band. d) Scattered NO(v=2) probed via the γ_{02} band. Intensities are corrected for differences in laser pulse energy, $f(I_v)$, and MCP gain, Γ_v. The spectra b) c) and d) are used to calculate the absolute excitation probabilities.

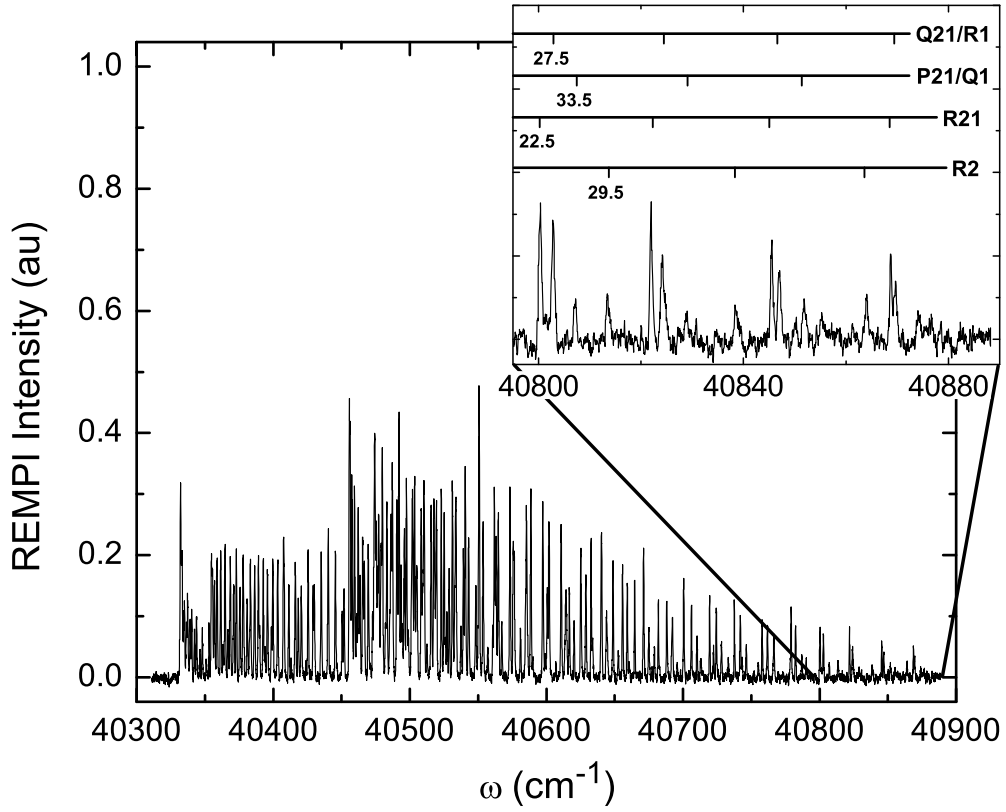

Figure 3: Absence of overlapping bands in the REMPI detection of scattered NO. (1+1) REMPI of scattered NO(v=2) at E_i=0.63eV and T_s=1000K. The inset shows the spectral region of γ_{02} where overlap with the band-head of γ_{13}, the nearest overlapping REMPI band, is expected. The comb in the inset indicates four branches in the γ_{02} band. All observable peaks can be assigned to high J states of the γ_{02} band.

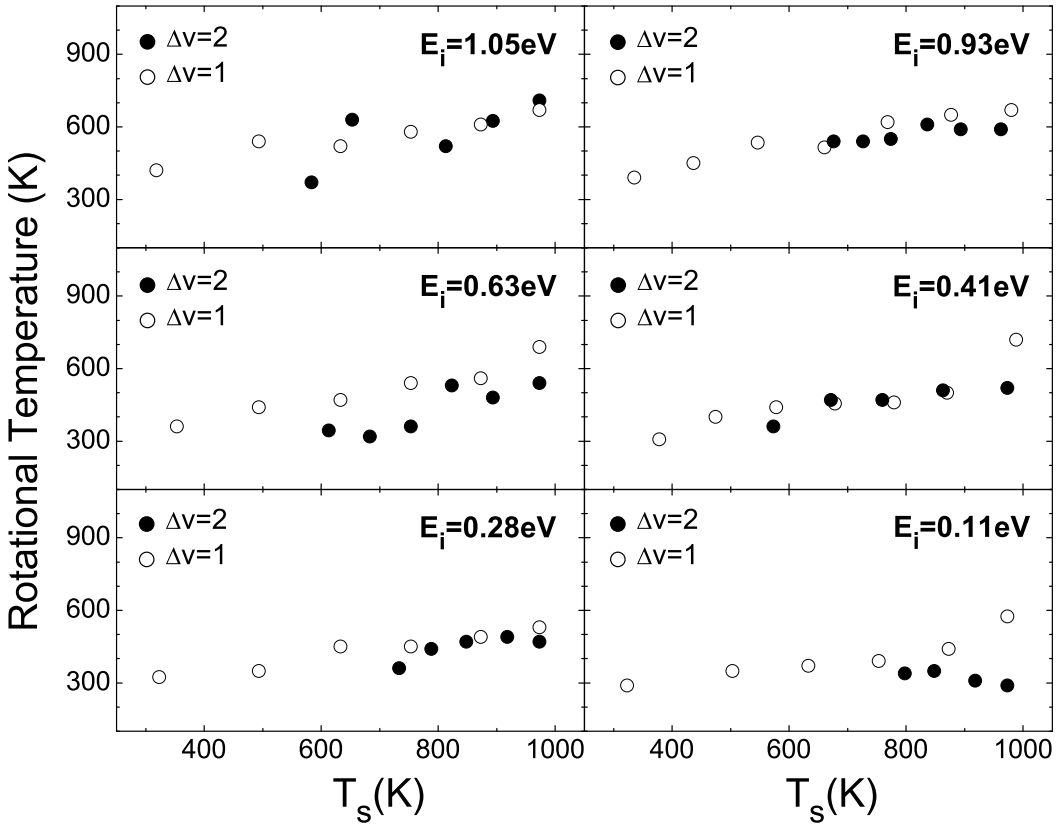

Figure 4: <u>Rotational temperature of NO molecules that have undergone the (v=0→1), empty circles, and NO(v=0→2), filled circles, transitions as a function of surface temperature at six different incidence energies of translation.</u> The rotational temperature is weakly dependent on surface temperature and incidence energy of translation.

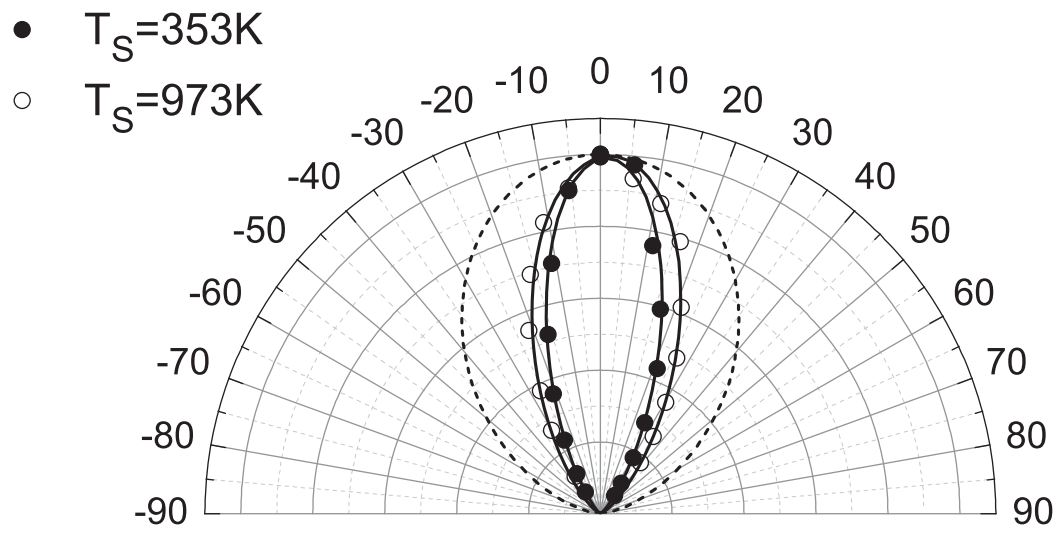

Figure 5: Angular distributions are weakly dependent on T_S. Angular distributions of NO molecules that underwent the v=0→1 transition at two surface temperatures filled circles, T_S=353 K and empty circles, T_S=973K) at E_i=0.93 eV. Gaussian fits to the two angular distributions are shown as black curves. The dashed line shows a $\cos(\theta)^2$ function for comparison.

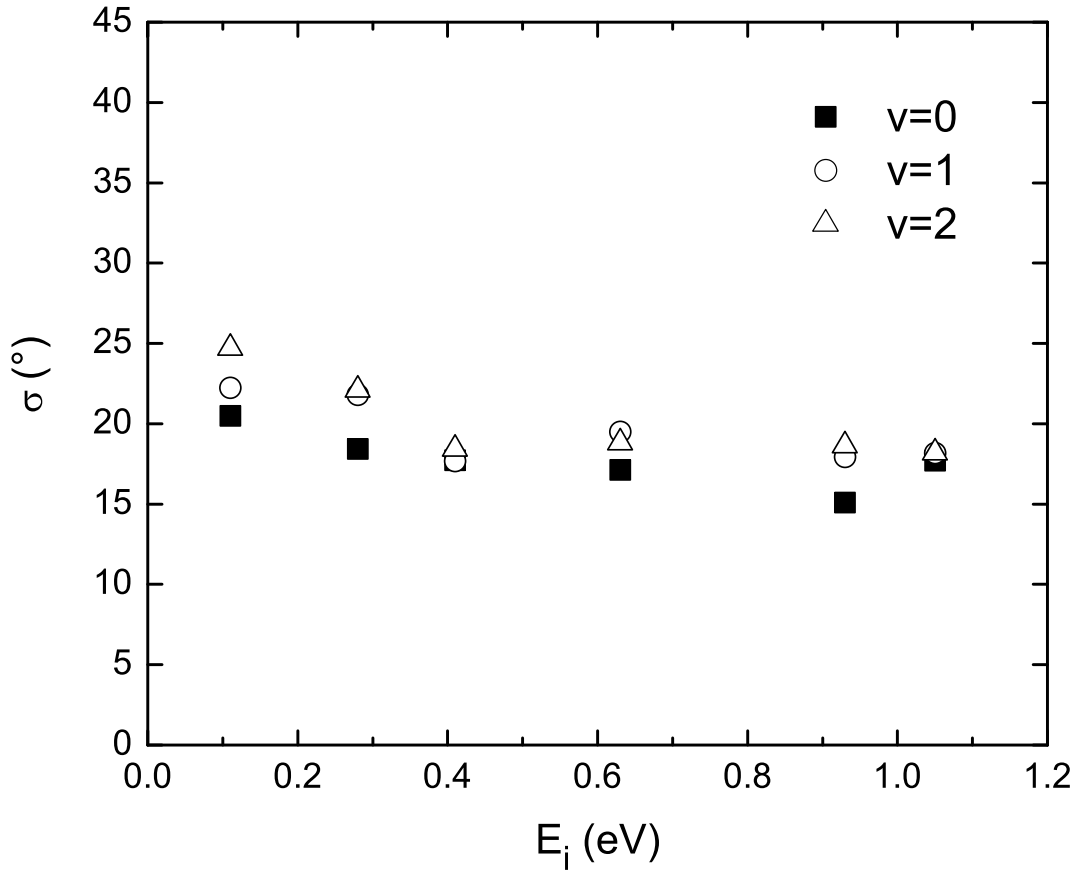

Figure 6: The width parameters of the angular distributions are only weakly dependent on incidence energy of translation and final vibrational state. Vibrationally elastic scattering NO(v=0→0) filled squares with T_s=300K, as well as vibrationally excited molecules, NO(v=0→1), empty circles, and NO(v=0→2), open triangles at T_s=1000K . The width parameters refer to Eq. 8. See also Appendix A.

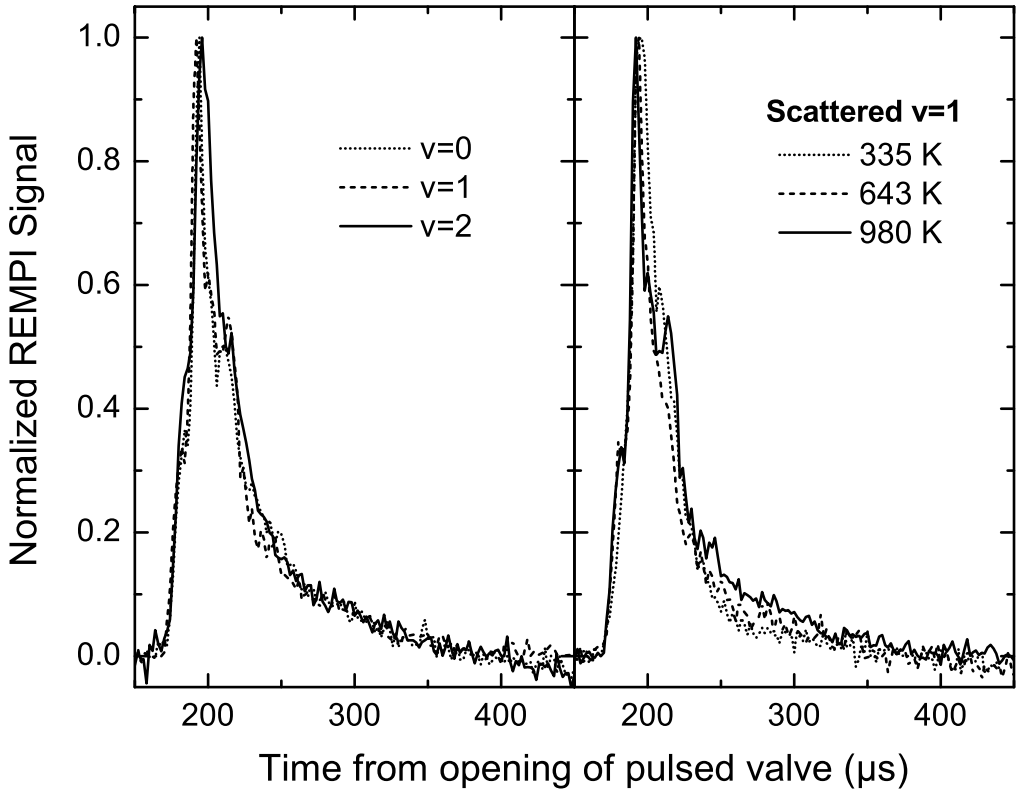

Figure 7: <u>Scattered delay time profiles are weakly dependent on final vibrational state and surface temperature</u>. The left panel shows delay time profiles dependence on final vibrational state, NO(v=0) dotted, NO(v=1) dashed, NO(v=2) solid at E_i=0.93eV. Delay time profiles for NO(v=0) were recorded at T_s=300K, while for NO(v=1) and NO(v=2), they were recorded at T_s=~1000K. The right panel shows the effect of surface temperature (T_s=335 K, dotted, T_s=643 K, dashed, and T_s=980 K, solid) on the delay time profile of scattered v=1 at E_i=0.93eV.

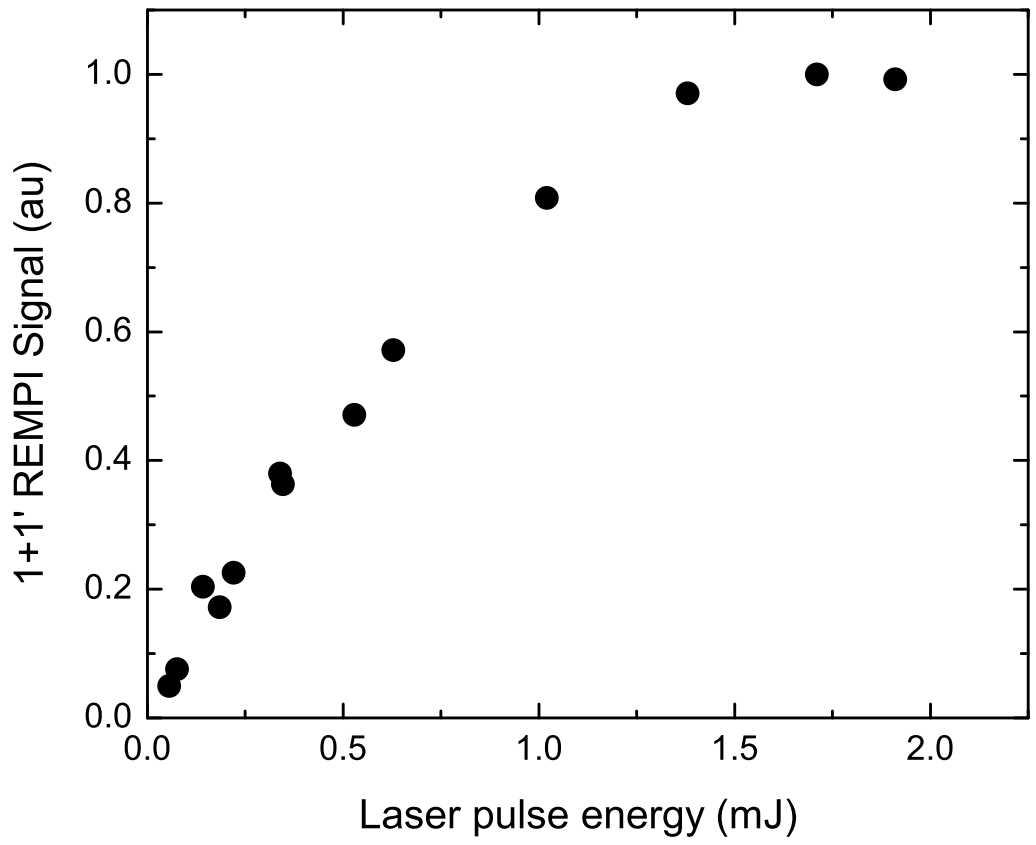

Figure 8: Saturation of the resonant step is shown by two-color (1+1′) REMPI of scattered NO(v=1) via the γ_{01} band. Here the resonant step taken employed laser pulse energies from 0.1 to 2mJ at ~230nm. This pulse energy is much lower than that of the 266 nm pulse (24 mJ) used for the ionization step. Hence the intermediate electronically excited state is predominantly ionized by the 266nm light. This laser pulse energy dependence therefore indicates the degree of saturation in the resonant step.

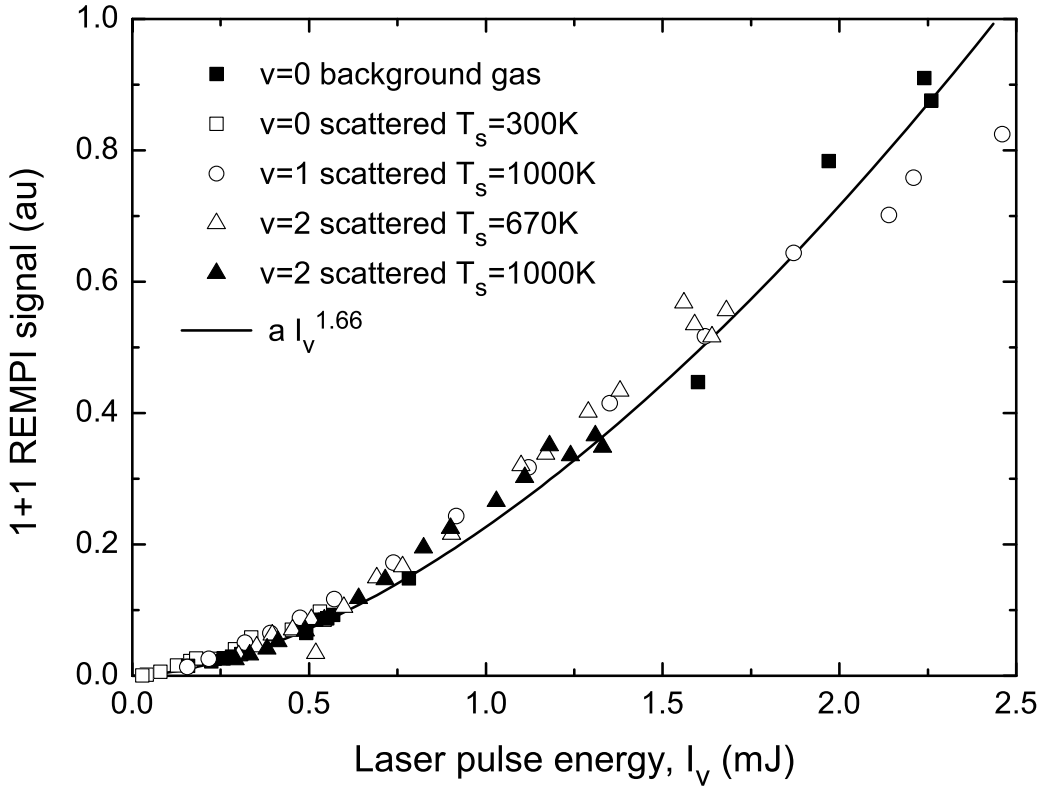

Figure 9: Laser pulse energy dependence of the (1+1) REMPI signal for NO in various vibrational states. REMPI signals were detected in the $\gamma_{0,v''}$ bands. The data shows a quadratic laser pulse energy dependence at low laser pulse energies, which becomes linear around 1 mJ/pulse, indicating saturation of the resonant step. The data is well described by the empirical laser pulse energy dependence, $f\ (I_v) \propto I_v^{1.66}$, shown as a solid line.

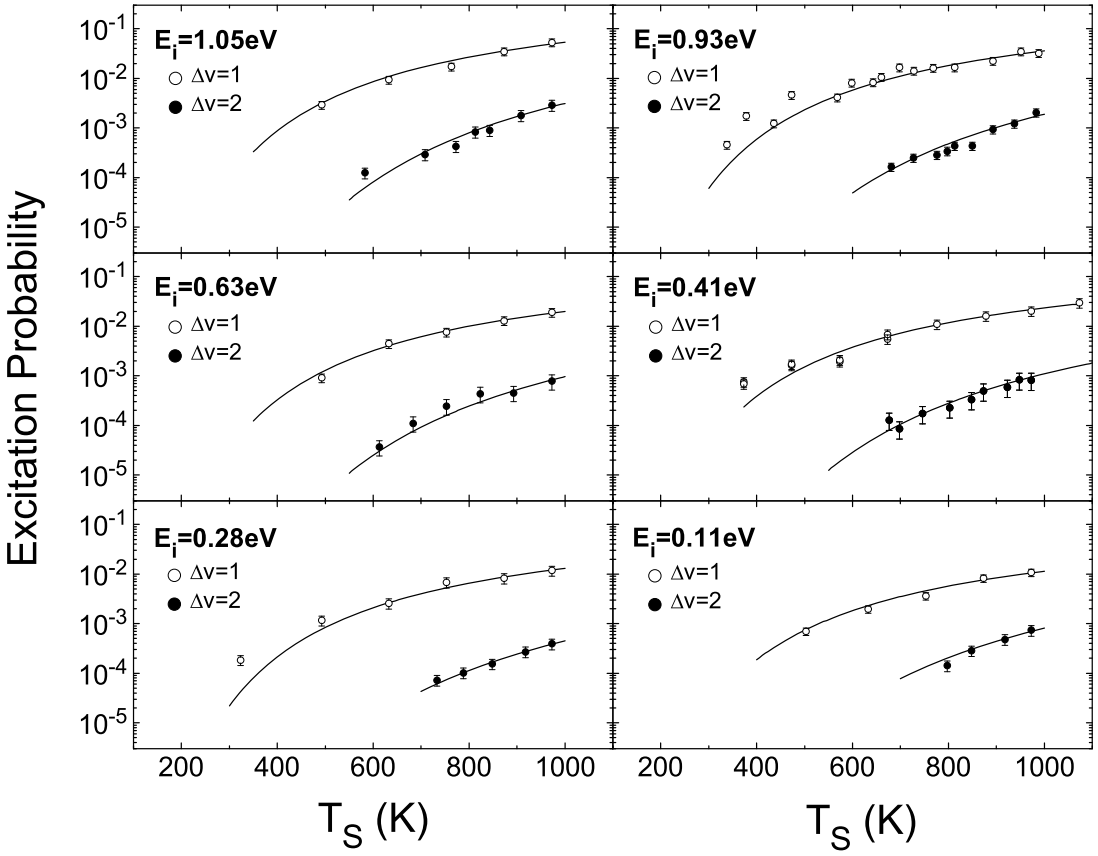

Figure 10: <u>Vibrational excitation probabilities for NO(v=0→1), empty circles, and for NO(v=0→2), filled circles, measured as a function of surface temperature for six different incidence energies</u>. The solid lines are Arrhenius fits with the activation energy fixed to the vibrational energy transferred.

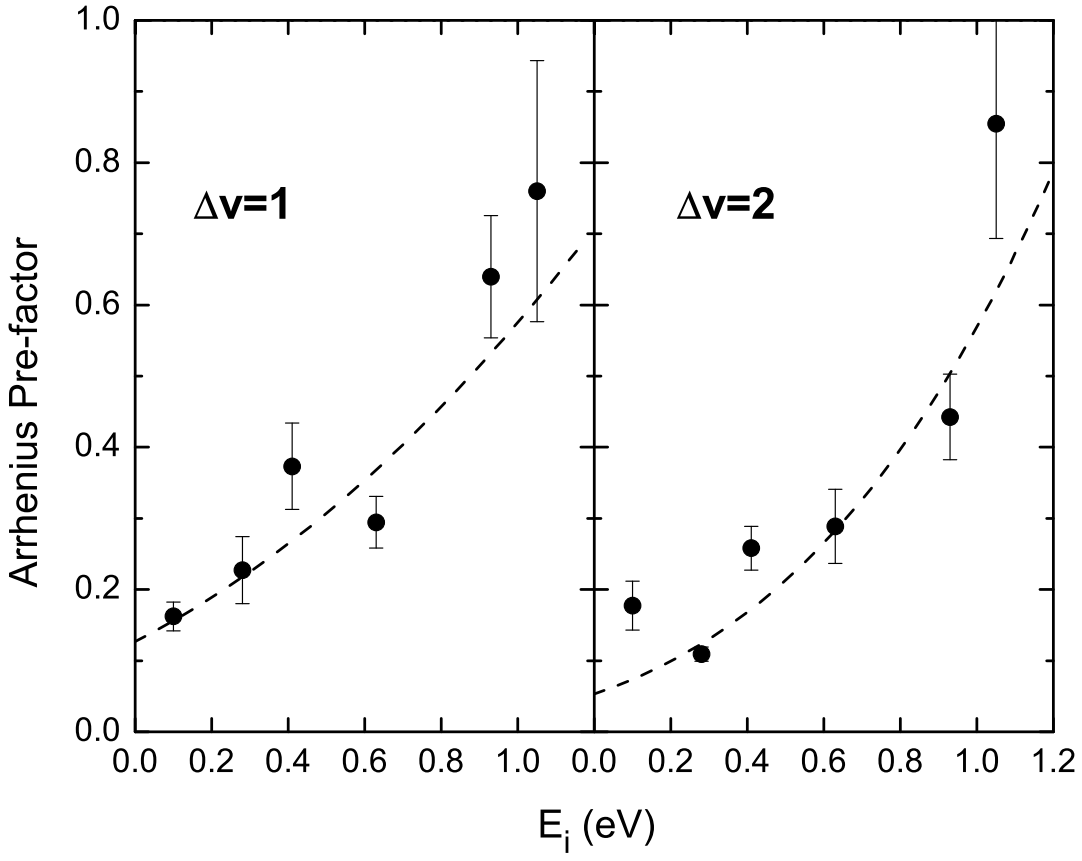

Figure 11: <u>Arrhenius pre-exponential factors dependence on incidence energy of translation</u>. Left panel NO(v=0→1); right panel NO(v=0→2). The error bars represent the 90% confidence interval. The dashed line is an aid to guide the eye. The pre-exponential factor reflects the intrinsic electronically nonadiabatic coupling that induces vibrational excitation.

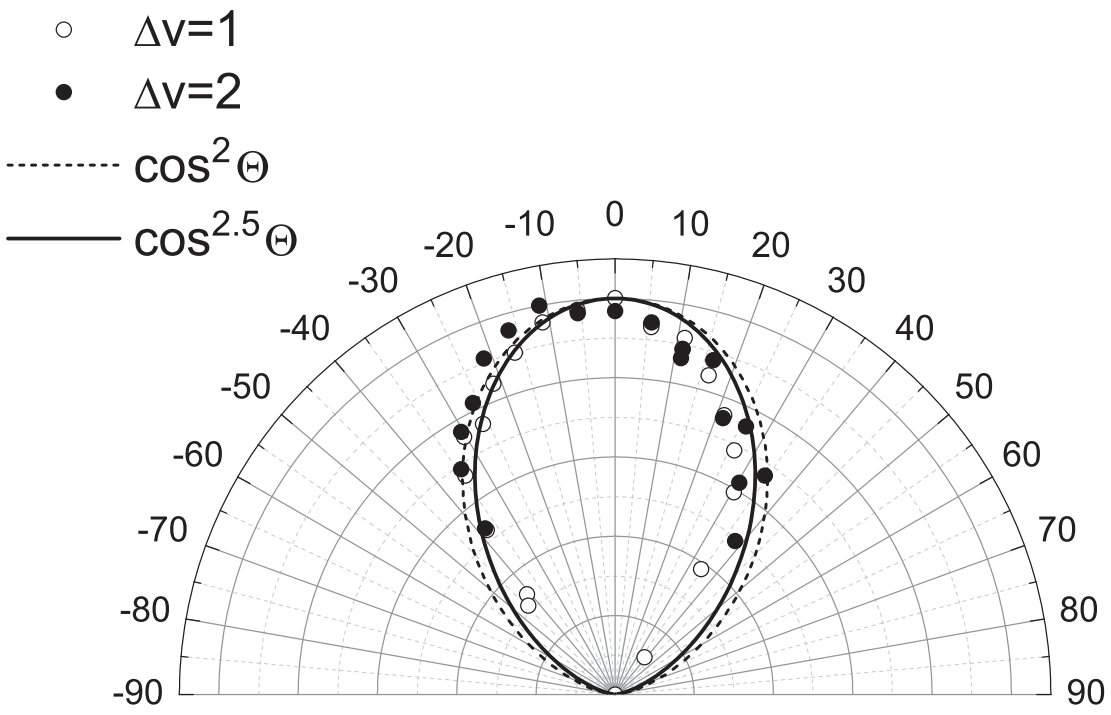

Figure 12: Angular distributions for NO(v=0→1), empty circles, and NO(v=0→2), solid circles for E_i=0.11eV and T_s=1000K. The angular distribution is quite wide, virtually indistinguishable for trapping desorption, dashed line.